Density-functional theory and atomistic simulation of the hard-sphere melt-solid interface

Agathagelos Kyrlidis* and Robert A. Brown
Department of Chemical Engineering, Massachusetts Institute of Technology, Cambridge, Massachusetts 02139
(Received 30 October 1994)

The melt-solid interface of hard spheres is studied by atomistic simulations and density-functional theory (DFT). The Monte Carlo method is used to compute density profiles for the three most important orientations of the fcc-solid–melt interface. The interface ranges in thickness from $4d$ for the loosely packed (110) interface to $6d$ for the closely packed (111) interface, where d is the hard-sphere diameter. The planar generalized effective liquid approximation (PGELA) free energy functional, which accurately predicts solid and liquid free energies and coexistence conditions, is used in the DFT analysis of the hard-sphere melt-solid interface. Two parametrizations are compared for variations of the density in the interfacial region. The structural predictions of the interface by the Carnahan-Starling PGELA are in good agreement with the simulations. The calculations of the surface free energies show that the (110) interface has a smaller surface free energy, followed by the (100) interface and then closely by the (111) interface. These results are compared to other recent studies of the hard-sphere melt-solid interface.

PACS number(s): 61.20.Gy, 64.70.Dv, 64.60.Cn

I. INTRODUCTION

The melt-solid interface plays a very important role in the determination of properties of crystals grown from the melt. When the solidification rate is zero or very small, the interface is in equilibrium. Then the interface is fully characterized by its microscopic structure, its thermodynamic properties, and its effect on dynamic properties, such as the diffusivity of solutes in this region. This paper focuses on the prediction of the structure and thermodynamic properties for an interface at equilibrium. The effect of the melt-solid interface on dynamic properties has been recently reviewed by Laird and Haymet [1]. The kinetics of crystal growth and of nonequilibrium solidification at the melt-solid interface are also very important, but are beyond the scope of this work; the reader is referred to Ref. [2] for discussion of these topics.

The melt-solid interface has not been studied experimentally to the extent of the solid-gas or the liquid-gas interfaces, despite its importance in the nucleation and growth of crystals from the melt and other phenomena involved in the processing of materials. The focus of most experimental studies has been the direct or indirect measurement of the solid-melt interfacial free energy. There is no experimental information on the structure of the melt-solid interface. In contrast to solid surfaces, where techniques, such as low-energy electron diffraction and Auger spectroscopy, allow direct structural analysis of the interfacial region [3], it has been impossible to apply these methods to the study of a surface confined between two dense phases that interfere with the probing radiation.

Theoretical modeling of the melt-solid interface has evolved significantly. A review of the advances in the development of these theories is given by Woodruff [2]. Most theories are concerned with the *structure* of the melt-solid interface. The most famous theory for the equilibrium melt-solid interface was developed by Jackson [4] and is extremely simple. It is built on a two-level model, where only nearest-neighbor bonds are considered, and is based on a simplified Bragg-Williams statistical model. Surprisingly, the behavior of many materials follows this simple model, although there are a few exceptions [2]. The notion that the interface can extend at the most to two layers is extremely simplistic. To remedy that, Temkin [5] proposed a theory that considers the interface as a region consisting of layers that include both solid and liquid atoms and uses the number of layers as the key variable to be adjusted in the minimization of the overall free energy of the system. This model reduces to the Jackson theory in the limit of a two-layer surface. Besides these important structural models, there have been a few *nonstructural* theories dealing with the calculation of γ_{SL}. Most notable are the broken bond models, which sum up energies associated with "broken" or "dangling" bonds in the crystal due to the absence of similar atoms on the liquid side of the interface. These theories either associate with the broken bond a suitable portion of the binding energy of each atom in the solid or use an interatomic potential with the help of one or more adjustable parameters [6–8].

Clearly, what is lacking in all these models of the melt-solid interface is the consistency provided by a framework such as classical density-functional theory. Density-functional theory (DFT) provides the flexibility to study the coexistence of the solid and the liquid phases, is not limited by the local inhomogeneities in the interface, and provides both structural and thermodynamic information.

All DFT approaches for modeling the melt-solid interface begin with calculations of the solid-liquid coexistence conditions. These studies of the melt-solid inter-

*Present address: Molten Metal Technology, Inc., 421 Currant Road, Fall River, MA 02720.

face have followed advances in the development of flexible and accurate free energy functionals. Another equally important feature in approximations of the interfacial region is the type of density parametrization that is used to describe the interfacial variation of the density.

To describe inhomogeneous solids Haymet and Oxtoby [9] introduced the concept of a spatially varying order parameter. In a perfect crystal the order parameter is fixed to its bulk value. In an inhomogeneous solid (for example, in the melt-solid interface, near a dislocation, or near a grain boundary) the density variations in the solid are written as

$$\rho(\mathbf{r})=\rho_0[1+\mu_0(\mathbf{r})]+\rho_0\sum_n \mu_n(\mathbf{r})e^{i\mathbf{k}_n\cdot\mathbf{r}}, \quad (1)$$

where the $\{\mathbf{k}_n\}$ represents the set of reciprocal lattice vectors of the crystalline lattice and $\{\mu_n(\mathbf{r})\}$ is the set of spatially varying order parameters. The order parameters describe all the inhomogeneity in the system and vary spatially; e.g., they depend on one space dimension in the modeling of an interface. Oxtoby and Haymet [10] used this approach in the study of bcc (100) and (110) interfaces with the melt and modeled the variation of the order parameters in the interfacial region by a square gradient approximation (SGA). Using a very small number of reciprocal lattice vectors they predicted the interfacial region to be very broad, with a width of approximately 10–15 layers, and justified *a posteriori* the validity of the SGA.

The SGA has also been used by Shih *et al.* [11] in a Landau-Ginzburg theory for the melt-solid interface. This approach yields a tractable mathematical description that was used to estimate the interfacial free energy for Si and Ge melt-solid interfaces [12], but yields only isotropic estimates, and is not based on a self-consistent prediction of freezing. Zeng [13] adopted the SGA and assumed a functional form for the order parameters. Using just one order parameter, Zeng obtained reasonable results for alkali metals. Moore and Raveche [14] applied a perturbative free energy functional in conjunction with the very simple parametrization for the interface, $\rho(\mathbf{r})=\rho_l+\psi(z)[\rho_s(\mathbf{r})-\rho_l]$, coupled with a square gradient approximation for the variation of ψ. This was not a self-consistent theory of freezing, because simulation values for the coexistence properties of the Lennard-Jones (LJ) potential were used as input. They obtained interfaces with unrealistic structures and a broadness of approximately 15 layers. They also found a large degree of anisotropy in the surface free energies, with γ_{SL} for the (111) orientation being a factor of 3 above the value for the (100) orientation. These predictions are at odds with the results of atomistic simulations.

An alternative variational approach was examined by McMullen and Oxtoby [15,16] using the same perturbative DFT free energy functional employed in [14]. They assumed a functional form for the variation of the order parameters throughout the interface similar to that used by Zeng [13] and kept a subset of the $\{a_n\}$ as independent variational parameters. A density parametrization without any peak broadening led to nearly isotropic surface free energies of $\gamma_{SL}d^2/kT\approx 1.7$. Introducing peak broadening led to density profiles in closer resemblance to those obtained from simulations and led to an increase in the surface free energy to $\gamma_{SL}d^2/kT=4$ [16].

All the theories described above use the perturbative DFT free energy functional. Also, a number of these add the square gradient approximation, which cannot be justified. The broadness of the interface should not be input into the model, but should be predicted as a consequence of the analysis. Curtin [17] first attempted such predictions using the Percus-Yevick (PY) hard-sphere melt-solid interface and the weighted density approximation (WDA) nonperturbative free energy functional. The square gradient approximation was avoided through the use of a flexible parametrization of the interfacial density. Curtin [18] predicted that the (111) and (100) interfaces have similar widths, each spanning approximately four layers. The surface free energies of the (111) and (100) interfaces were computed as $\gamma_{SL}d^2/kT=0.63\pm0.02$ and 0.66 ± 0.02, respectively. The ordering of the magnitudes of these surface free energies is in contrast to the simulation results of Broughton and Gilmer for the LJ system [19].

The large computational effort required to study the interface using the method of Curtin inspired Marr and Gast [20] to develop a planar formulation of the WDA free energy functional, introducing a one-dimensional weighted density that captures the local free energy variations across the interface. The savings are significant that result from reducing the dimensionality of the weighted density. Marr ang Gast used this functional in the study of the (111) PY hard-sphere interface and found results very similar to those of Curtin. The thickness of the (111) interface was predicted to be approximately 3–4 layers, while the surface free energy was calculated to be $\gamma_{SL}d^2/kT=0.60\pm0.02$.

The analyses of Curtin [17,18] and Marr and Gast [20] use the relatively inaccurate PY thermodynamic and structural functions for the description of the high-density uniform liquid properties required in the DFT [21]. We present results for the planar generalized effective liquid approximation (PGELA) free energy functional, which yields very accurate predictions for both the free energies and the solid-liquid coexistence conditions for a hard-sphere system described by the Carnahan-Starling (CS) equation of state and the Baus-Colot direct correlation function [22]. The ability to approximate well both phases leads to conditions of coexistence that are closer to the real hard-sphere system.

A series of Monte Carlo (MC) simulations were performed to investigate the structure of the hard-sphere melt-solid interface; these simulations are presented in Sec. II. The density-functional theory for the hard-sphere melt-solid interface is presented in Sec. III and is compared to previous DFT analyses. Emphasis is given to the parametrization of the interface and the accuracy of the free energy functional used in the DFT. Results are presented for the (111), the (100), and the (110) hard-sphere melt-solid interfaces. The results are compared to the MC simulation predictions and discussed in Sec. IV.

II. SIMULATIONS OF THE MELT-SOLID INTERFACE

Atomistic simulations of the equilibrium melt-solid interface (for reviews see [1,23,24]) have been performed for a wide variety of systems ranging from water [25] to semiconductor materials [26,27]. Simulations have also been reported for nonequilibrium melt-solid interfaces in an effort to model either laser annealing [28] or growth under supercooling conditions [29]. The most widely studied system using atomistic simulations is the melt-solid interface of the Lennard-Jones potential [30–34]. The most complete study of this interface was presented by Broughton and Gilmer [19,35], who compared the (111), the (110), and the (100) interfaces at the triple point of the LJ system. They found that the intrinsic widths of these interfaces were quite similar, approximately 3σ. The density oscillations propagated further into the liquid phase for the close-packed (111) and (100) interfaces. The most important contribution of this work was the development of an accurate method for the direct calculation of the excess interfacial free energy γ_{SL} through simulations; unfortunately, this method has not found wider application because of its computational intensity.

The hard-sphere system has been studied less thoroughly, even though it is a very important system for the development of theoretical models for the melt-solid interface. Surprisingly, there have been no true simulations of the hard-sphere melt-solid interface, with the only study of this system using the Bernal model for the structure of liquids.

The Bernal model [36] is essentially a static, random close-packing description of the hard-sphere liquid. It describes a liquid as being a *heap* of molecules, containing no inherent regular structure, and manages to predict qualitatively the pair distribution function and enthalpies of phase transformations. This model has been studied both experimentally, using either ball bearings [36,37] or ping pong balls [38], and through computer simulation [23]. Zell and Mutaftschiev [39] built a physical model of the melt-solid interface by packing 2000 ping pong balls in a container to generate the random packing necessary to represent the liquid and then placed the model in contact with a plane with close-packed hexagonal structure representing the crystal face. The coordinates of the spheres were logged and a density profile across the interface was measured. The difficulties in this study and the lack of precision of the coordinate measurements inspired Bonissent and Butaftschiev [40] to construct a computer model for the same system.

Both of these studies support the conclusion that the melt-solid interface is relatively narrow—about 3 atomic diameters wide—and that there is a substantial density deficit in the layers of the liquid adjacent to the solid face [23]. These results have been shown to be an artifact of the static nature of the Bernal model [34,41], which also was limited by the lack of any relaxation of the particles comprising the solid wall in contact with the liquid [40].

The lack of true atomistic simulations for the hard-sphere melt-solid interface has motivated the work described in this section. Our goal is to generate density profiles for the three major orientations of this interface. To do this requires the formulation of a simulation of a hard-sphere interface without using the static packing techniques of Bonissent and Mutaftschiev. The Monte Carlo simulation described below overcomes this limitation.

Simulation formulation and results

The details of a hard-sphere Monte Carlo simulation are discussed in Ref. [42]. There are some considerations for a melt-solid interface simulation that are worth noting. First, coexistence must be ensured for the solid and the liquid phase. Second, a starting configuration must be generated that brings the two phases together without overlap of the particles. Third, the interface should be stationary during the simulation, otherwise the density profiles will be artificially broadened.

The solid density is set to the coexistence value $\rho_s d^3 = 1.041$ determined by Hoover and Ree [43]. The solid phase is constructed layer by layer according to the orientation of the face that is exposed to the liquid. Generating the liquid in contact with the crystal is somewhat more complicated. In simulations of soft potentials, such as the LJ potential, it is possible to take a liquid simulated at the required bulk density and temperature and then brings it in contact with the solid phase. In the hard-sphere case, this requires more effort. A liquid configuration at the coexistence density $\rho_l d^3 = 0.943$ must be generated that does not overlap with the given structured crystal surface. This step can be accomplished by using a Bernal model for the hard-sphere liquid against the crystal face [40] by either generating a liquid configuration for a higher density, removing all particles that overlap with the crystal particles and removing more particles until the coexistence density is achieved, or by melting a crystalline region at the liquid coexistence density that is in contact with the face.

In this work, a perfect crystal at the solid coexistence density first is generated from a specified number of layers in the x, the y, and z directions, as described previously. This ensures the matching of the size of the simulation cells for the solid and the liquid phases. The simulation cell is assembled by bringing the liquid blocks in contact with the crystal, in the way illustrated in Fig. 1. Then $(\rho_s - \rho_l)V$ particles are removed from the liquid blocks. This can be done in one of two ways.

(i) Particles can be randomly removed from the block effectively creating a very high concentration of vacancies in the crystal, which induces melting. The difference between the coexisting densities of the solid and the liquid phase for a hard-sphere system is approximately 10%.

(ii) Particles from the layers of the liquid block that are in contact with the crystal faces are removed. In principle, this step is equivalent to suddenly expanding the crystal by 10%.

Both of these methods were tested and found to lead to the melting of the liquid blocks after approximately 100 000 MC sweeps, during which the solid block was

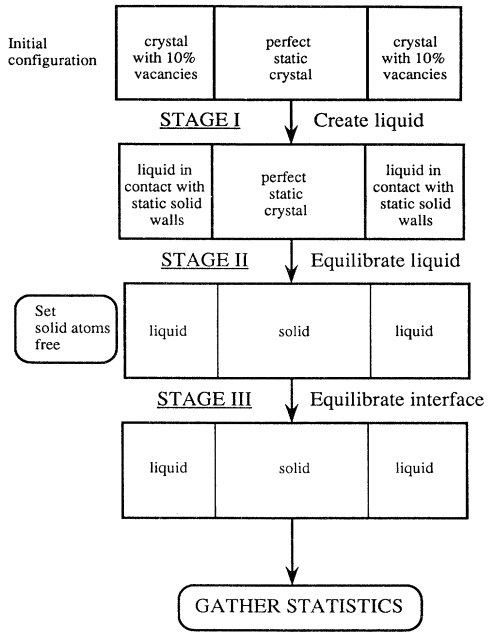

FIG. 1. Algorithm for constructing the cell for the MC simulation of the hard-sphere melt-solid interface.

held fixed. This configuration is then equilibrated for another 100 000 MC sweeps.

The procedure used is equivalent to performing a Monte Carlo simulation for a dense hard-sphere fluid confined between structured crystal walls. Calculations of hard-sphere fluids against or confined between structureless hard walls have been performed to study the wetting properties of the hard-sphere fluid [44,45]. None of these simulations have produced results for liquids with densities $\rho_l d^3 > 0.91$ because of the difficulty in generating an initial configuration. One of the problems with this method is that in the (N-V-T) Metropolis MC simulation only the number density of the simulation cell can be controlled and not the "bulk" liquid density. In this case the liquid absorbs on the structured crystal walls, thereby reducing the bulk liquid density to approximately $\rho_l d^3 = 0.93$. This behavior also was observed by Snook and van Megen [46].

The plane averaged density profile for the melt-solid interface is generated by dividing the z direction of the simulation cell into 1000 bins, counting the number of particles in each of these bins throughout the simulation, and averaging for the total number of sweeps as

$$\rho(z_i) \equiv \langle N(z_i) \rangle / V_{\text{bin}} , \tag{2}$$

where z_i is the position of the ith bin, V_{bin} is the volume of the bin, and

$$N(z_i) = \sum_{i=1}^{N} \hat{\delta}(z - z_i) , \tag{3}$$

where $\hat{\delta}$ is defined as

TABLE I. System size parameters used in Monte Carlo simulations of the melt-solid interface.

Parameter	(111)	(100)	(110)
$N_l(x)$	8	12	18
$N_l(y)$	10	12	14
$N_l(z)$	18	20	20
$N_l(z)$ fixed	6	8	8
N_s total	1440	1440	1260
N_s fixed	480	576	504
N_l total	1740	2610	2284

$$\hat{\delta}(z - z_i) \equiv \begin{cases} 1 & \text{if } z_i - \dfrac{\Delta z_b}{2} \le z \le z_i + \dfrac{\Delta z_b}{2} \\ 0 & \text{otherwise} , \end{cases} \tag{4}$$

where Δz_b is the width of the bin in the z direction.

The parameters used in the simulations are given in Table I. Periodic boundary conditions were used in all three spatial dimensions, in a simulation cell with a rectangular xy cross section. The density profiles for the three interface orientations at the end of the first stage of the simulations are shown in Fig. 2. The three profiles are similar, but quantitatively different.

The liquid in contact with the (111) crystal face, which is the most closely packed orientation, has a structure

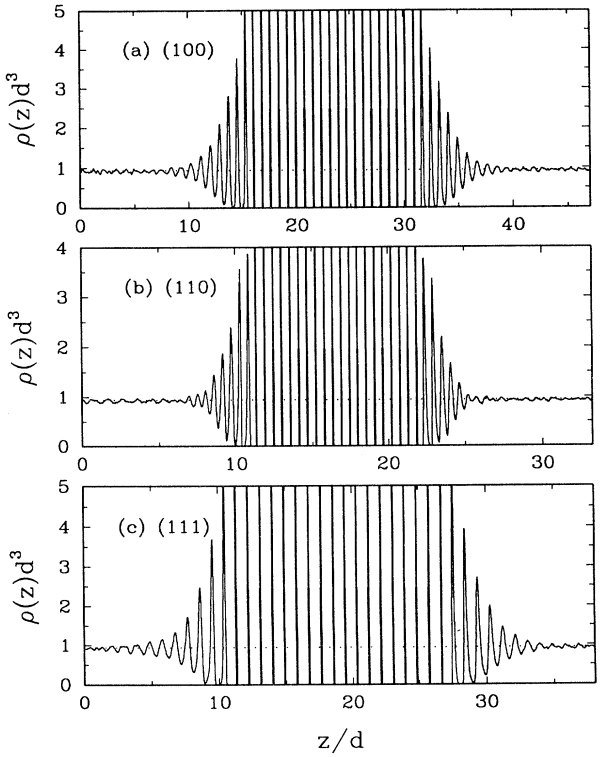

FIG. 2. Density profile computed after stage II of the MC simulation of the hard-sphere melt-solid interface, for interfaces in the (a) (100), (b) (110), and (c) (111) crystallographic orientations exposed to the melt.

that persists for approximately $5d$. The liquid that is against the (110) crystal face is less structured. Approximately the same number of layers is formed (in all three cases there are about 5–6 peaks in the oscillation of the liquid density as it approaches the wall) because the spacing between the layers in the (110) direction is smaller; however, the structure of the wall propagates through a smaller region of the liquid. For all three orientations, the first layer is distinctly crystalline in nature, as can be seen from the peak in the density. In the case of a hard-sphere liquid at the coexistence density against a structured wall, the first layer adopts the structure of the static solid substrate. In contrast, when a hard-sphere is against a hard featureless wall the first layer assumes the closest-packed (111) triangular lattice configuration, as is inferred from the lattice spacing in the molecular dynamics study of hard-sphere wetting by Courtemanche and van Swol [47].

After the equilibration of the hard-sphere liquid in contact with the static crystal with the desired orientation, the particles designated as solid are allowed to move. After 50 000 equilibration steps, we start averaging over the entire simulation cell to generate the desired density profiles. This period is as important as stage 2 because it allows the solid layers to relax to their equilibrium bulk configurations. The mean density of the "bulk" liquid phase was seen to rise during this stage, approaching the "exact" liquid coexisting density of $\rho_l d^3 = 0.943$, thereby indicating that the interface is indeed in equilibrium.

It is important to avoid translations of the bulk of the simulation cell, which could lead to broadening of the density peaks and to a flattening of the interface. To prevent this the center of mass is shown in Table I for the three interfaces. This constraint is much softer than keeping static solid layers and should not affect the predictions for the density profiles across the interface. This constraint was imposed by first calculating the center of mass of the N_s "fixed" particles, computing the displacement from their static center of mass, and then by rescaling *all* particle positions by this displacement. This corresponds essentially to translating the bins at every sweep in order to guarantee that the bulk solid phase does not translate.

Before the density profiles are discussed, the effect of the soft constraint on the interface profiles is investigated. Bonissent, Gauthier, and Finney [48] allowed only two solid layers to be mobile, thus restricting the interfacial thickness and affecting the interfacial density calculations [41]. The effect of the constraint used here was studied by short simulations for the (100) interface in which all particles were moved freely, to mimic molecular dynamics calculations in the melt-solid interface [19]. Averages were taken over 5000 sweeps, in which time the translation of the center of mass of the central eight layers was $\delta x = 0.046$, $\delta y = 0.024$, and $\delta z = 0.028$; these movements are very small compared to the spacing of the layers, which is $\delta_{100} = 0.783$ for the (100) interface. The two interfaces are compared in Fig. 3. Other than larger fluctuations in the liquid density, which are expected because the averages were constructed over a smaller number of sweeps, the density profile of the unconstrained simulation is very similar to that of the original simulation; the constraint imposed has little effect on the density profiles other than allowing the simulation to run for a larger number of sweeps without any translation of the crystal.

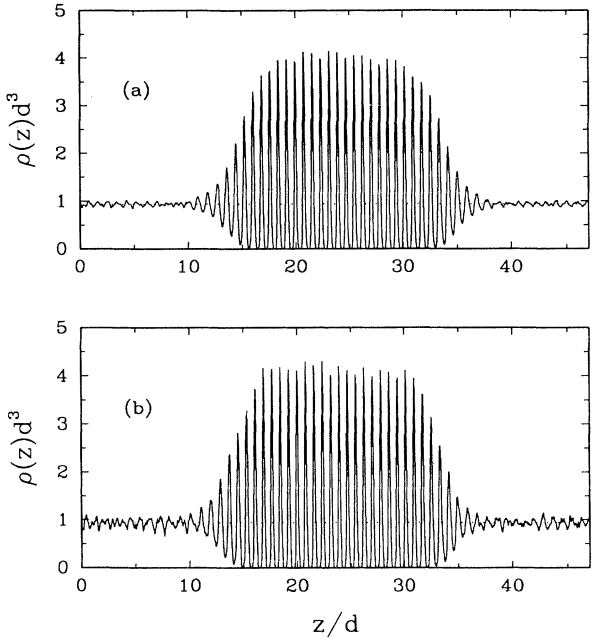

FIG. 3. Comparison of (100) interface profiles generated by (a) a simulation where the center of mass of the central eight layers of solid was held fixed for 50 000 sweeps and (b) a simulation where all particles were allowed to more freely for 5000 sweeps.

Three simulations, one for each crystallographic orientation, describe the hard-sphere melt-solid interface because no effects of temperature need to be considered. The density profiles for the (100), the (110), and the (111) interface orientations are shown in Fig. 4 after averaging over 50 000 sweeps. Once again, the interfaces have some similar and some distinctive features.

The (100) interface is the most interesting. The interface width is approximately six layers. The first two layers are spaced with a separation of $\delta_{100} = 0.783$, which corresponds to the (100) spacing. The layers tend to relax outward and the period of the density oscillations in the liquid changes to that of the (111) spacing ($\delta_{111} = 0.905$), as shown in Fig. 5. This observation is similar to one previously reported in the literature for a LJ system [19,34]. This feature is very difficult to approximate with density parametrizations of the melt-solid interface, as is discussed further in Sec. III. The total width of the interface based on the density variations is approximately $(4-5)d$ for the (100) interface.

The (111) interface has the most structure. As in the case of the liquid against the static structured crystal face, this is not entirely unexpected because the (111) face is the most tightly packed. The interface width is approximately 5–7 layers. The spacing of the peaks of the density oscillations remains constant at its bulk solid value, until the peaks decay and become indistinguishable

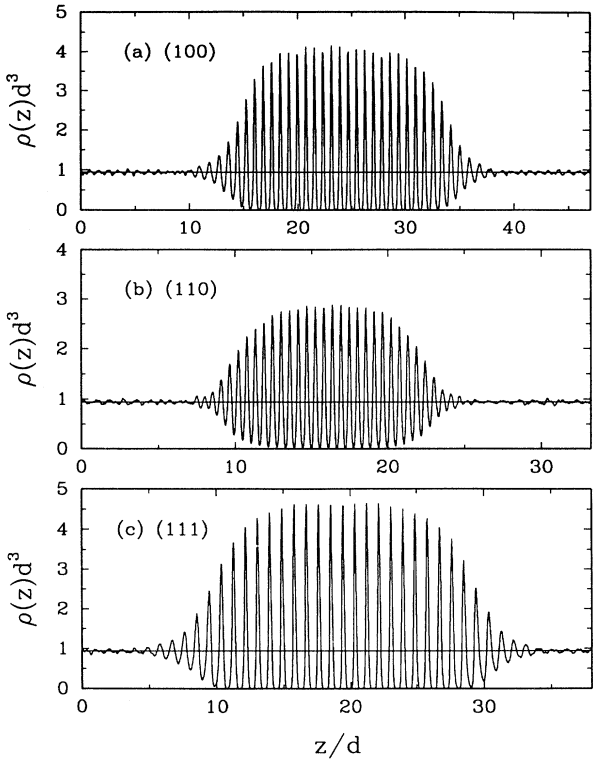

FIG. 4. Melt-solid interface density profiles for (a) (100), (b) (110), and (c) (111) orientations of the crystal face exposed to the melt.

from the noise in the liquid density. The width of this interface is about $(5-6)d$.

The (110) interface has some unique features. The spacing of the peaks in the density oscillations remains equal to the bulk solid separation of $\delta_{110}=0.554$. The transition from bulk to bulk liquid involves slightly more layers than for the (100) and the (111) interfaces; the width is approximately 8–9 layers or $4d$. The height of the density peaks is smaller because of the open structure of this crystalline surface. This difference also causes the faster damping of the density oscillations in the liquid side as compared to the (111) interface.

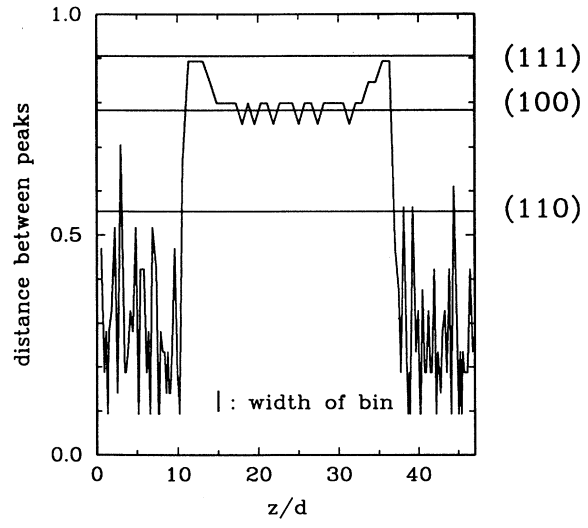

FIG. 5. Transition from (100) to (111) spacing of layers in the (100) melt-solid interface.

The density profiles in this work are very similar to the LJ melt-solid interfaces simulated by Broughton and Gilmer [19] and the larger simulations of Galejs, Raveche, and Lie [49] for the LJ system. This is not too surprising because the melt-solid interface structure is in a large part determined by the repulsive core of the interatomic potential.

III. DENSITY-FUNCTIONAL THEORY OF THE HARD-SPHERE MELT-SOLID INTERFACE

A. PGELA study of the melt-solid interface

The basic principles of DFT are described in [50] and will not be repeated here. Several excellent review papers have been published that review its variations and applications [51–54]. The Helmholtz free energy F functional of the inhomogeneous system is written as

$$F[\rho]\equiv F_{\rm id}+F_{\rm ext}+F_{\rm ex}\ , \tag{5}$$

where this functional is the sum of three contributions.

(i) The *ideal gas* contribution $F_{\rm id}$ corresponds to the limit of no interparticle interactions

$$F_{\rm id}=\beta^{-1}\int d\mathbf{r}\,\rho(\mathbf{r})\{\ln[\rho(\mathbf{r})\Lambda^3]-1\}\ , \tag{6}$$

where $\Lambda\equiv(h^2\beta/2m\pi)^{1/2}$ is the thermal wavelength.

(ii) The *external potential* contribution $F_{\rm ext}$ corresponds to the effects of external forces acting on the system

$$F_{\rm ext}=\int d\mathbf{r}\,\rho(\mathbf{r})W(\mathbf{r})\ . \tag{7}$$

(iii) The *excess* free energy contribution $F_{\rm ex}$ corresponds to the contributions to the free energy that are due to the interatomic interactions in the system.

The first two terms are known exactly as functionals of the nonuniform system density $\rho(\mathbf{r})$ as given by Eq. (6) and (7). The excess free energy functional is unknown and various density-functional approximations differ in the construction of approximations to this term. Models for $F_{\rm ex}[\rho(\mathbf{r})]$ cause the distinction between perturbative and nonperturbative approximations. Perturbative density-functional approximations are based on an expansion of the properties of the inhomogeneous system around those of a uniform liquid, which is well characterized by liquid state theory [9]. The limited success [55] of this approach led to the development of a whole family of approximations that *avoid* using Taylor series expansions about the uniform liquid. Nonperturbative approximations to the excess free energy are constructed based on the definition of the two-body direct correlation function of inhomogeneous systems $c^{(2)}(\mathbf{r}_1,\mathbf{r}_2)$ as the second functional derivative of the excess free energy with respect to the density. The excess free energy is written as [56]

$$\beta F_{\rm ex}[\rho]=-\int d\mathbf{r}\int d\mathbf{r}'\int_0^1 d\lambda(1-\lambda)\rho(\mathbf{r})\rho(\mathbf{r}') \times c^{(2)}(\mathbf{r},\mathbf{r}';[\lambda\rho]) , \quad (8)$$

which is an exact expression for the excess free energy of an inhomogeneous system. Unfortunately, it requires the knowledge of $c^{(2)}(\mathbf{r},\mathbf{r}')$, which is unknown. Approximations for $c^{(2)}(\mathbf{r},\mathbf{r}')$ cause all nonperturbative DFTs to be inexact. Various approximations are based on thermodynamic and structural information of the uniform liquid, which is either available in analytical form (i.e., for the hard-sphere system) or may be computed from atomistic simulations or integral equation theory.

The first of the two approximations is the *thermodynamic* mapping approximation, which has origins that may be traced back to Van der Waals [57]. Both global [56,58] and local [59,60] forms of this approximation have been determined and differ according to the symmetries in the inhomogeneous system. We focus on the approximations that are used in the systems where the bulk density varies in one spatial dimension, otherwise known as the planar mapping approximations. The excess free energy is written as

$$F_{\rm ex}[\rho(\mathbf{r})]=\int d\mathbf{r}\,\hat{\rho}(z)f_0(\bar{\rho}(z)) , \quad (9)$$

where $\hat{\rho}(z)=(1/A)\int dx\,dy\,\rho(\mathbf{r})$ is the plane-averaged density introduced by Marr and Gast [20].

Several different prescriptions for the structural mapping have been used. We use the structural mapping

$$\int d\mathbf{r}\int d\mathbf{r}'\rho(\mathbf{r})\rho(\mathbf{r}')c^{(2)}(\mathbf{r},\mathbf{r}';[\rho]) = \int d\mathbf{r}\int d\mathbf{r}'\rho(\mathbf{r})\rho(\mathbf{r}')c^{(2)}(|\mathbf{r}-\mathbf{r}'|;\bar{\rho}(z;[\rho])) , \quad (10)$$

which maps the density weighted direct correlation function of the inhomogeneous system to the density weighted direct correlation function of the effective system with density $\bar{\rho}(z)$ at each point along the z direction [61]. This is the basis of the PGELA.

The DFT introduces three unknowns: the excess free energy $\beta F_{\rm ex}$, the two-body direct correlation function $c^{(2)}(\mathbf{r},\mathbf{r}')$, and the effective (or weighted) density $\bar{\rho}(z)$. These variables are determined from three equations: the exact equation (8) and the thermodynamic and structural mapping equations (9) and (10). Combining these equations yields a framework for the evaluation of the free energy of the inhomogeneous system so that the equilibrium density of the nonuniform system is found by minimizing the total free energy F with respect to the density profile $\rho(\mathbf{r})$.

The study of coexistence of a hard-sphere solid with a liquid using the PGELA free energy functional is described in [62]. The results of this study are used as the starting point for the analysis of the melt-solid interface. Specifically, the information that is required for the PGELA model is listed in Table II.

The application of density-functional theory to melt-solid interface focuses on the calculation of the excess interface thermodynamic properties. The grand potential Ω for the inhomogeneous interfacial region is expressed as

TABLE II. Comparison of coexistence properties predicted by the PGELA and the PWDA [20] density-functional theories to melt-crystal system simulations, where $\Delta\rho=\rho_s-\rho_l$ and $P=\beta p d^3$ is the pressure.

Theory	$\rho_s d^3$	$\rho_l d^3$	$\Delta\rho/\rho_s$	P
MC	1.04	0.94	0.094	11.7
PGELA (PY)	1.001	0.904	0.097	10.5
PWDA (PY)	1.026	0.882	0.140	9.5
PGELA (CS)	1.038	0.945	0.089	11.9

$$\Omega[\rho(\mathbf{r})]=F[\rho(\mathbf{r})]-\mu\int d\mathbf{r}\,\rho(\mathbf{r}) . \quad (11)$$

At solid-liquid coexistence conditions,

$$\Omega_s=-PV_s,\quad \Omega_l=-PV_l , \quad (12)$$

so that the excess grand potential of the melt-solid interface becomes

$$\Delta\Omega[\rho(\mathbf{r})]=F[\rho(\mathbf{r})]-\mu\int d\mathbf{r}\,\rho(\mathbf{r})+PV , \quad (13)$$

where $V=V_s+V_l$ if $V_{\rm int}=0$. According to the variational principle of DFT [50], the interfacial region is described by a density profile $\rho(\mathbf{r})$, which minimizes $\Delta\Omega$, subject to the constraints that the region is surrounded by the bulk phases, i.e., $\rho(\mathbf{r})=\rho_s(\mathbf{r})$ and $\rho(\mathbf{r})=\rho_l$ at the coexistence values of (μ,P,T). The excess interfacial free energy is given as

$$\gamma_{\rm SL}=\left[\frac{\Delta\Omega}{A}\right]_{\rm min} , \quad (14)$$

where the subscript implies that the value of the excess grand potential corresponds to the minimum.

The following steps are needed to proceed with the calculation of $\gamma_{\rm SL}$.

(i) A density parametrization for $\rho(\mathbf{r})$ is defined, which introduces a set of variational parameters $\{a_n\}$.

(ii) The ideal contribution to the free energy of the inhomogeneous interfacial region is computed.

(iii) The excess contribution to the free energy from the PGELA free energy functional is computed. This involves solving for $\bar{\rho}(z)$ at every integration point across the interface.

(iv) The computed value of $\Delta\Omega$ is minimized with respect to the set of variational parameters $\{a_n\}$.

The accuracy and the efficiency of the parametrization used to describe the density variations in the interfacial region plays important roles in the utility of a DFT for the melt-solid interface. For example, McMullen and Oxtoby [15,16] demonstrated significantly different predictions for the surface free energy $\gamma_{\rm SL}$ using two different parametrizations of the surface and shed doubt on the accuracy of the square gradient approximation for predicting interface structure.

The efficient parametrization of $\rho(\mathbf{r})$ in the interfacial region is a challenging problem. The approximation must evolve smoothly between the densities of the surrounding bulk solid an liquid phases, using a minimal set of parameters. The atomistic simulations described in

Sec. II suggest functional forms and discount others. For example, the approximation used by Moore and Raveche [14] is not optimal because it does not allow for any broadening of the peaks in the density across the interface, as is observed in the density profiles shown in Fig. 4. The approximation to the density profile should capture the gradual broadening of the peaks across the interfacial region, which leads through eventual overlaps to a uniform liquid density. Predictions of the rate of broadening of the peaks and the width of the interfacial region should result from the free energy minimization for the inhomogeneous system and should not be fixed by the parametrization.

Curtin developed a flexible representation of the interfacial density [18] using two variables. The starting point was the parametrization of Haymet and Oxtoby [9] [Eq. (1)] rewritten as

$$\rho(\mathbf{r})=\rho_l+(\rho_s-\rho_l)h_0(z)+\sum_{\mathbf{G}}\rho_G h_G(z)\exp(i\mathbf{G}\cdot\mathbf{r}) , \quad (15)$$

where $\{\rho_G\}$ are the coefficients of the Fourier expansion for the Gaussians used to represent the density variations in the bulk solid and $\{h_G\}$ is a set of *shape* functions that characterize the transition between the solid and the liquid across the interface. The shape functions must satisfy

$$\begin{aligned} &h_G(z)\to 1 \quad \text{as } z\to\text{solid} , \\ &h_G(z)\to 0 \quad \text{as } z\to\text{liquid} \end{aligned} \quad (16)$$

to match the bulk values of the density. Curtin used the following expression to describe the shape functions:

$$h_G(z)=\begin{cases} 1, & |z|<z_0 \\ \frac{1}{2}\left\{1+\cos\left[\pi\left[\dfrac{z-z_0}{\Delta z_G}\right]\right]\right\}, & z_0<|z|<z_G \\ 0, & z_G<|Z| , \end{cases} \quad (17)$$

where z_0 is the starting point of the interface, $z_G=z_0+\Delta z_G$ is the point where the shape function obtains its liquidlike value, and Δz_G is the width of the interface. Equation (17) gives the shape function corresponding to a slab geometry with two equivalent melt-solid interfaces.

If all shape functions were allowed to decay on the same length scale, there would be no broadening of the density peaks across the interfacial region. To incorporate peak broadening, Curtin assumed that the decay rate of the shape functions is determined by the magnitude of the corresponding reciprocal lattice vector G, so that the decay length is given by

$$\Delta z_G=|z_G-z_0|=(G_1/G)^{\nu}\Delta z, \quad 0\le\nu\le 1, \quad G\ge G_1 , \quad (18)$$

where G_1 is the magnitude of the smallest nonzero reciprocal lattice vector, the parameter $\Delta z=\Delta z_0$ controls the width of the interface, and the parameter ν controls the rate of broadening of the density peaks.

The parameters $\{\Delta z,\nu\}$ are the two variables in the parametrization, Eqs. (15)–(18). This approach has the following advantage.

(i) The extent of the interfacial region is strictly defined through the parameters z_0 and Δz. This simplifies the integrations required to compute the excess interfacial properties.

(ii) The use of the slab geometry with two interfaces allows the computation of the Fourier transform of the shape function. This greatly simplifies the calculations of the weighted density.

A limitation of this parametrization (termed P-I) is that it truncates the density oscillations very suddenly in the liquid region. The atomistic simulations described in Sec. II showed that the density oscillations decay over longer length scales in the liquid. This is an effect of the use of the cosine function by Curtin. In this work, the Curtin parametrization is used as a reference because it has been used by most previous studies of the melt-solid interface using nonperturbative DFT [17,18,20].

To study the effect of the decay of the density oscillations in the liquid, we have developed an alternative density parametrization, which is similar to P-I, but does not restrict the end of the decay length z_G. This is achieved by constructing a hybrid parametrization

$$h_G(z)=\begin{cases} 1, & z<z_0 \\ \frac{1}{2}\left\{1+\cos\left[\pi\left[\dfrac{z-z_0}{\Delta z_G}\right]\right]\right\}, & z_0<z<z_0+\dfrac{\Delta z_G}{2} \\ \frac{1}{2}\left\{1-\tanh\left[\pi\left[\dfrac{z-z_0}{\Delta z_G}-\dfrac{1}{2}\right]\right]\right\}, & z_0+\dfrac{\Delta z_G}{2}<z \end{cases} \quad (19)$$

for a slab geometry about the origin and for positive values of z. The parametrization [Eq. (19)] (termed P-II) combines the advantages and flexibility of the Curtin parametrization with the decay of the hyperbolic tangent, which is more realistic for the interfacial region. The solid side of the interface begins at z_0. The shape functions decay to half of their value in the $\Delta z_G/2$ region and then decay smoothly to the liquid value. The only disadvantage of parametrization P-II with respect to the parametrization P-I is in the fact that the Fourier transforms of these shape functions cannot be performed analytically, which makes calculations with parametrization P-II more expensive.

Using the PGELA-DFT formulation the excess free energy of the interface region is given by the thermodynamic mapping equation

$$F_{\text{ex}}=A\int dz\,\hat{\rho}(z)f_0(\bar{\rho}(z)) , \quad (20)$$

where A is the surface area of the interface, $\hat{\rho}(z)=(1/A)\int dx\,dy\,\rho(\mathbf{r})$ is the planar averaged density, and $\bar{\rho}(z)$ is the weighted density.

The weighted density is given by the PGELA equation

$$-\beta f_0(\hat{\rho}(z))=\frac{\int dx\,dy\,\rho(\mathbf{r})\int d\mathbf{r}'\int_0^1 d\lambda(1-\lambda)c_0^{(2)}(|\mathbf{r}-\mathbf{r}'|;\bar{\rho}(z;[\lambda\rho]))}{A\hat{\rho}(z)} . \quad (21)$$

Equation (21) is a nonlinear integral equation for the $\bar{\rho}(z)$, which is solved at each integration point for the evaluation of the integral in Eq. (20).

The solution procedure used is similar to that used for the bulk solid and is the same as that presented by Lutsko and Baus [56] using the generalized effective liquid approximation. The integrals on the right-hand side of Eq. (21) are difficult to compute in real space, because they involve integrating over five spatial dimensions and one integration in λ. The density parametrization Eq. (15) is introduced into the set of equations to transform integrations in real space to sums over reciprocal lattice vectors. This transformation significantly reduces the number of arithmetic operations and is described extensively in Refs. [18,20,62].

The resulting equations are solved numerically using Newton's method, with the components of the Jacobian matrix evaluated by numerical differentiation. The weighted density profiles obtained this way should satisfy the requirements

$$\bar{\rho}_{\rm int}(z)\rightarrow\bar{\rho}_s(z),\ z\rightarrow\text{solid};\qquad \bar{\rho}_{\rm int}(z)\rightarrow\rho_l,\ z\rightarrow\text{liquid} \tag{22}$$

as tests of the accuracy of the approximation in the solution for $\bar{\rho}(z)$.

Given the weighted density profile, the excess free energy contributions are computed from Eq. (20). Gaussian quadrature is used in the integration over z. Some terms in the equations for $\bar{\rho}(z)$ are divided by the plane-averaged density $\hat{\rho}(z)$. In the interlayer space, this quantity becomes very small and affects the accuracy of the solutions for $\bar{\rho}(z)$. In the calculations that follow, all integration points at which $\hat{\rho}(z)\leq 10^{-3}$ are ignored. Marr and Gast [20] used a similar convention to avoid convergence problems in their planar weighted density approximation (PWDA) treatment of the melt-solid interface.

The excess grand potential for the interfacial region is evaluated and minimized with respect to $(\Delta z,\nu)$. Because of the computational cost in the evaluation of $\Delta\Omega$ the minimization is carried out with the two parameters sequentially. The sensitivity of the predictions to the two variational parameters is described in Sec. III B.

B. Results of DFT analysis

The PGELA-DFT formulation of the melt-solid interfacial region was used to calculate the (100), the (110), and the (111) melt-solid interfaces for the hard-sphere system, using the PY and the CS equations of state. The results for the CS hard-sphere system are presented in Sec. III B 1 with both the P-I and the P-II density parametrizations. Results for the PY system also are presented in Sec. III B 2 in order to compare the predictions of the PGELA with those of previous density-functional approximations for the hard-sphere melt/solid interface.

1. *Carnahan-Starling hard spheres*

The variation of the surface free energy $\gamma_{\rm SL}$ with the width of the interface Δz is shown in Fig. 6 for the (111) interface. The results use the two parametrizations P-I and P-II, for a fixed value of the rate of broadening $\nu=0.25$, which was found by Curtin [18] to correspond to the minimum surface free energy in the WDA study of the interface. The width parameter is scaled by the bulk solid layer spacing $\delta_{111}=a/\sqrt{3}$. Both the P-I and the P-II parametrizations yield similar results, with the minimum in the surface free energy corresponding to an interface with a width of three layers. The minimum is steeper for the P-II parametrization. Relaxing the decay on the liquid side minimizes the excess free energy for narrower interfaces. The value of $\gamma_{\rm SL}$ predicted using the parametrization P-II for $\Delta z=2$ is significantly smaller than that predicted using the P-I parametrization. Near the minimum the effect becomes less important and for $\Delta z>3$ the relaxation has the opposite effect. The surface free energy is computed as $\beta\gamma_{\rm SL}d^2=0.37$.

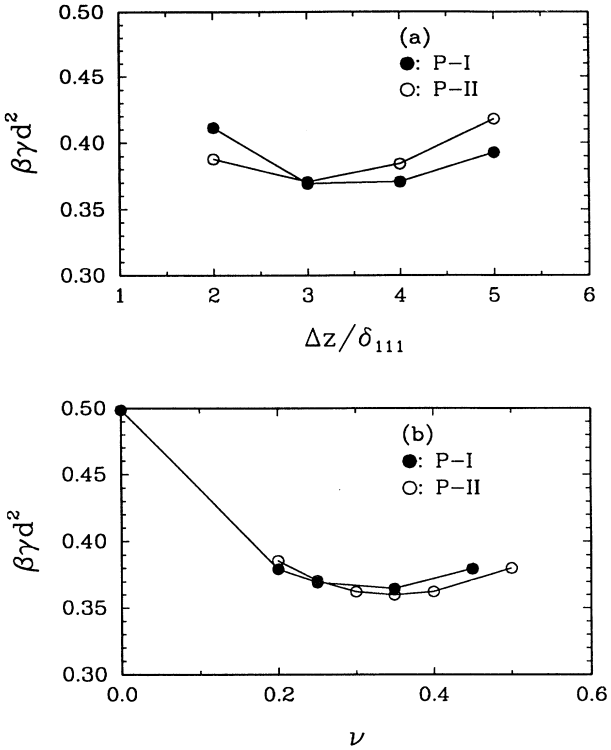

FIG. 6. (a) Variation of the surface free energy with the width of the (111) interface, for the P-I (●) and the P-II (○) density parametrizations with $\nu=0.25$. (b) Variation of the surface free energy with the parameter ν for the (111) interface, for the P-I (●) and the P-II (○) density parametrizations with $\Delta z=3$.

The equilibrium planar averaged density profiles predicted by the two parametrizations for the (111) interface are shown in Fig. 7. The results are identical in the first two layers, as expected; however, the P-II parametrization yields an interface with density oscillations that decay more slowly. This leads to a larger effective width for the interface. Using P-I the width of the interface is roughly $(3-4d)$. Alternatively, using the P-II parametrization there are at least two additional peaks in the

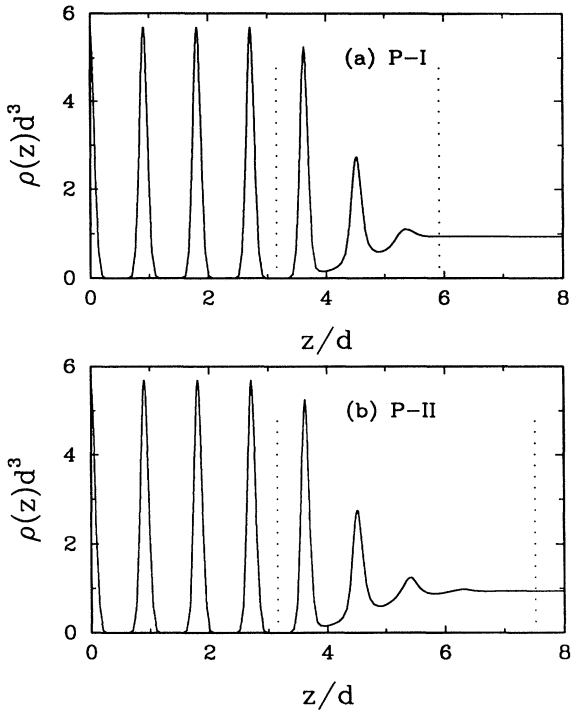

FIG. 7. Equilibrium planar averaged density profiles predicted by the PGELA for the (111) interface using the (a) P-I and (b) P-II density parametrizations. The dotted lines correspond to the boundaries of the interfacial region.

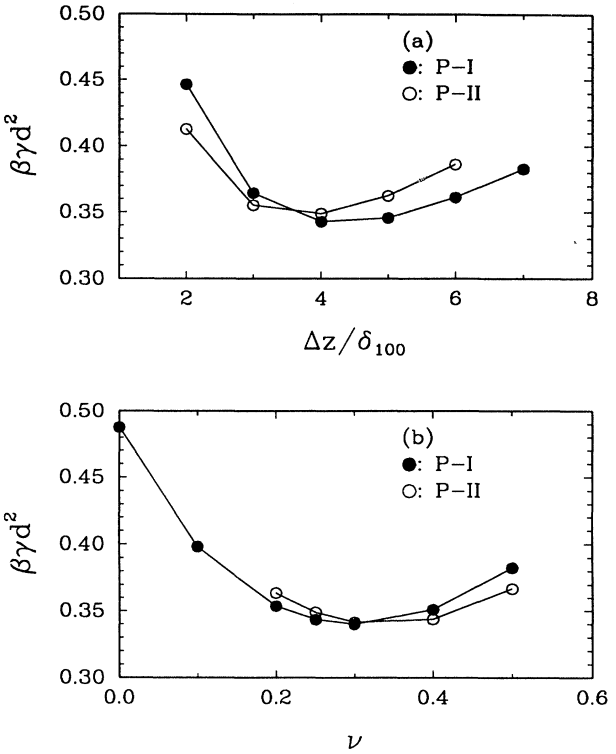

FIG. 8 (a) Variation of the surface free energy with the width of the (100) interface, for the P-I (●) and the P-II (○) density parametrizations with $\nu=0.25$. (b) Variation of the surface free energy with the parameter ν for the (100) interface, for the P-I (●) and the P-II (○) density parametrizations with $\Delta z=4$.

density, which increases the apparent width of the interface of $4.5d$. The MC simulations of Sec. II predicted an apparent width of $(5-6)d$ for the (111) interface. The theoretical predictions are thereby narrower than those computed by the MC simulation. The reason for this difference is unresolved; it is most likely due to shortcomings of the free energy functional or the parametrization.

The effect of modifying the parameter ν, which controls the rate of broadening, for a fixed value of $\Delta z=3$ is shown in Fig. 6 for the two density parametrizations P-I and P-II. The value of $\nu=0.25$ used for determining the minimum of the surface free energy with respect to the width of the interface lies very close to minimum, which for both parametrizations is around $\nu=0.35$. This difference in ν does not affect significantly the previous result for γ_{SL}. For the P-II approximation, the minimum value of the surface free energy is $\beta\gamma_{SL}d^2=0.36$.

Calculations for the (100) interface are reported in Fig. 8, which shows the effect of the interface widths on the surface free energy for $\nu=0.25$. For (100) orientation the spacing is $\delta_{100}=a/2$. The minimum of γ_{SL} lies at the value $\Delta z=4$. The corresponding values of the surface free energy are $\beta\gamma_{SL}d^2=0.34$ for P-I parametrization and $\beta\gamma_{SL}d^2=0.35$ for P-II parametrization. Unlike the results for the (111) interface, there is a small difference in the predicted values with the parametrization of the density. Again P-II parametrization is preferable for small Δz, but as $\Delta z>4$ its predictions for γ_{SL} become larger than those of P-I parametrization.

The planar averaged density profiles for the equilibrium interfaces are shown in Fig. 9 and are different from the MC simulations. In the case of the (100) interface both parametrizations are unable to capture the transition from the (100) layer spacing to the (111) layer spacing that was found in the MC simulations. This is because only structural information corresponding to the (100) interface orientation is used as input to the density parametrization.

The width of the interface predicted by P-I is again narrower than that predicted by P-II parametrization, for the same reasons as for the (111) interface. Specifically, the P-I parametrization yields the width of $\Delta z=3d$, while the P-II parametrization yields the slightly broader interface $\Delta z=(4-5)d$, in agreement with the MC simulations prediction. The variation of the surface free energy with the rate of broadening of the peaks for $\Delta z=4$ for both parametrizations is shown in Fig. 8. The behavior is very similar to the calculations for the (111) interface. The minimum for both parametrizations lies near $\nu=0.3$ and both parametrizations yield practically the same values for the surface free energy $\beta\gamma_{SL}d^2=0.34$.

The variation of γ_{SL} for the (110) interface orientation with the width of the interface is shown in Fig. 10, as measured in terms of the number of layers Δz. For the

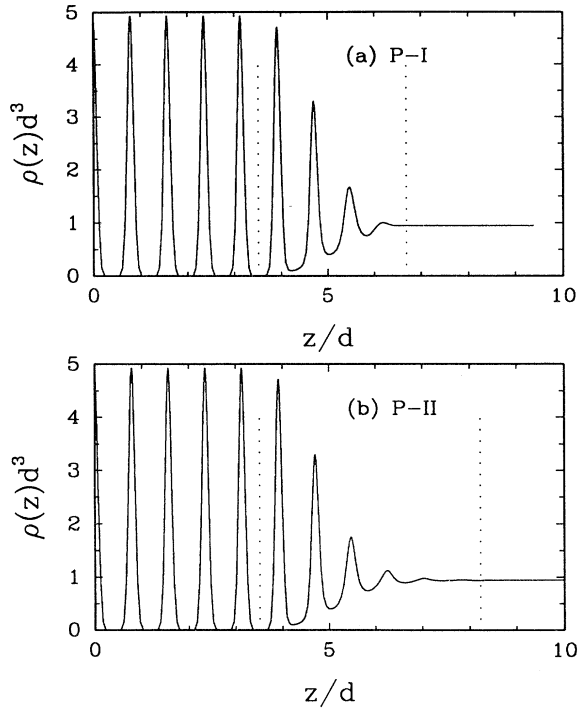

FIG. 9. Equilibrium planar averaged density profiles predicted by the PGELA for the (100) interface using the (a) P-I and (b) P-II density parametrizations. The dotted lines correspond to the boundaries of the interfacial region.

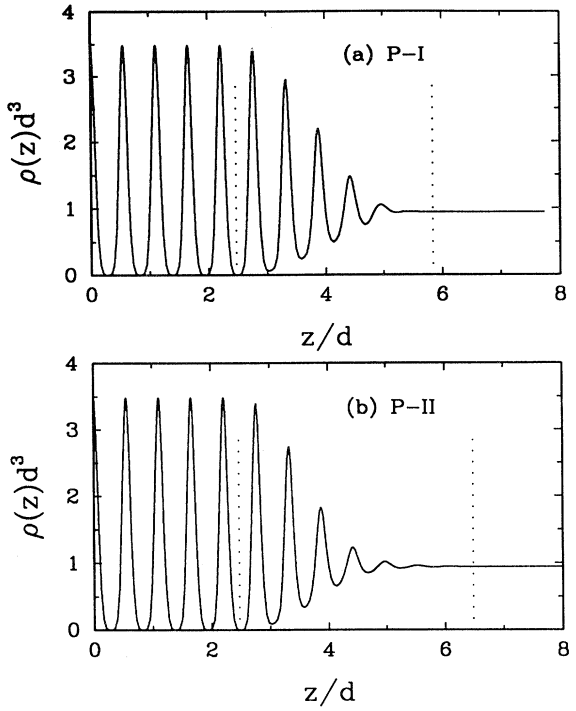

FIG. 11. Equilibrium planar averaged density profiles predicted by the PGELA for the (110) interface using the (a) P-I and (b) P-II density parametrizations. The dotted lines correspond to the boundaries of the interfacial region.

fcc (110) orientation, the width of each layer is $\delta_{110}=a/\sqrt{2}/4$. In this case, the two density parametrizations yield different minima; P-I has a minimum at $\Delta z=6$ with $\beta\gamma_{SL}d^2=0.32$ and P-II predicts a minimum at $\Delta z=5$ with $\beta\gamma_{SL}d^2=0.33$. The equilibrium planar averaged density profiles predicted for the two parametrizations are compared in Fig. 11. The interface predicted by P-I is narrower and has a width of $3.3d$; the interface predicted by P-II has a width of $4d$. The MC simulations predicted a width of approximately $4d$.

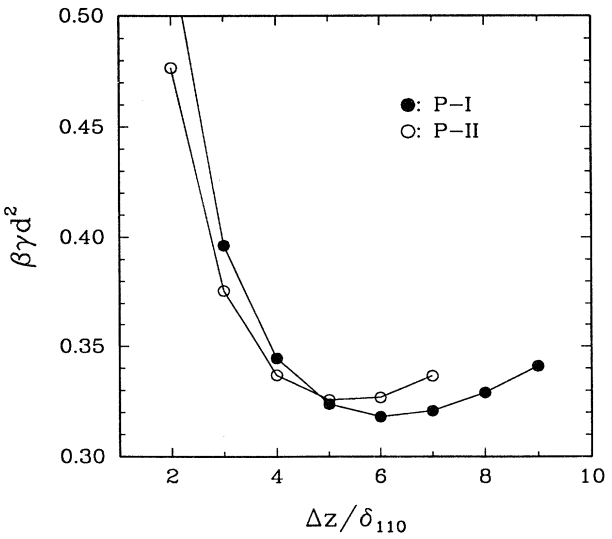

FIG. 10. Variation of the surface free energy with the width of the (110) interface, for the P-I (●) and the P-II (○) density parametrizations with $\nu=0.25$.

2. *Percus-Yevick hard spheres*

All the previous density-functional theory studies [15,16,18,20] of the hard-sphere melt-crystal interface have used thermodynamic and structural information for both the solid and the liquid phases from the Percus-Yevick equation of state and the corresponding Wertheim direct correlation function. The thermodynamic properties of the solid are not very sensitive to the information used because PY and CS solids have similar free energies. However, the liquid thermodynamic properties are quite sensitive to the equation of state and the coexistence conditions of a PY solid with a PY liquid are different from those predicted by atomistic simulations (see Table II). Both the solid and the liquid densities predicted by DFT for the PY system are lower than the exact values at coexistence and the solid is less structured.

Comparisons of the PGELA results to those of previous studies are based on results presented in Fig. 12 for the variation of γ_{SL} with the interfacial width for the (100), the (111), and the (110) interfaces for a value of $\nu=0.25$ in all calculations. Only the P-I parametrization was used in order to restrict the comparison to the effect of changing the free energy functional. The results do

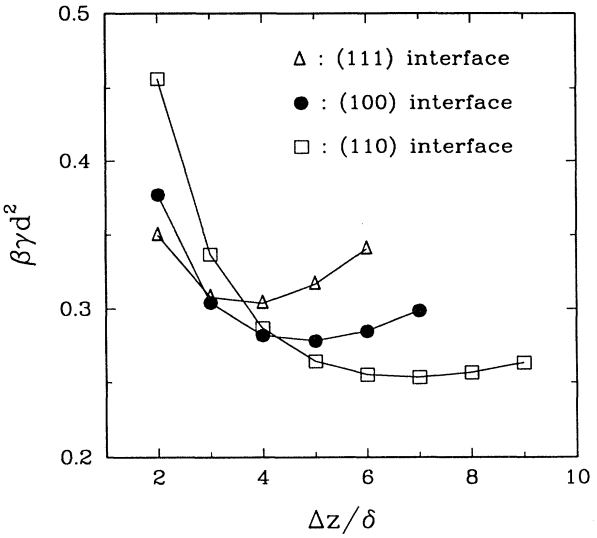

FIG. 12. Effect of the width of the interface Δz on the surface free energy γ_{SL} for PY hard spheres with $\nu=0.25$. Results for the (100) (●), the (111) (△), and the (110) (□) interface orientations.

not differ significantly from the predictions for the CS hard spheres. The (111) interface has an equilibrium width of four layers and $\beta\gamma_{SL}d^2=0.30$. Curtin [18] and Marr and Gast [20] both calculated similar widths for the (111) interface. However, both of these theories predicted a twice as large value for the (111) surface free energy. The (100) surface free energy is minimized at $\Delta z=5$ and gives $\beta\gamma_{SL}d^2=0.28$. The (110) interface again occupies the largest number of layers $\Delta z=6-8$ and gives $\beta\gamma_{SL}d^2=0.25$.

IV. SUMMARY AND DISCUSSION

The results of atomistic simulation and density-functional theory presented here give a thorough and self-consistent picture of the structure and energetics of the hard-sphere melt-crystal interface for the (100), the (110), and the (111) crystallographic orientations of the fcc crystalline structure. The Monte Carlo calculations predict the width of the interface to vary between $4d$ for the loosely packed (110) interface to approximately $6d$ for the more closely packed (111) interface. This variation is similar to calculations for continuous interatomic potentials [19]. These results supply an important point of comparison for the approximate DFT.

A density-functional theory for the melt-crystal interface was constructed by combining the PGELA free energy functional with two parametrizations of the density variation in the inhomogeneous melt-crystal system; one parametrization P-I was used by Curtin and others [17,18,20] and the second P-II is a variation of P-I. The results based on the Carnahan-Starling and the Percus-Yevick equations of state for the hard-sphere liquid are compared in Table III with the results for atomistic simulations and previous DFT approximations for the melt-crystal system. The structural predictions of the P-II–PGELA formulation based on the CS equation of state are in good agreement with the atomistic simulations, whereas the result using the P-I approximation give a somewhat narrower interfacial region, although the thermodynamic properties are similar to those predicted by the P-II parametrization. Thereby, the effects of the extended decay of the density implemented in the P-II parametrization are small.

The results in Sec. III B clearly indicate that the accuracies of the structural and thermodynamic properties depend on the accuracy of the parametrization of the density profile across the interface. Both parametrizations give plane-averaged density profiles in reasonable agreement with the simulation. However, other features of the simulation results, such as the variation in the spacing of the density peaks with distance for the (100) interface, are not captured by the parametrization used in this paper. Mikheev and Trayanov [63] have presented a more complex approximation of the density across the interface, which divides the region into two layers; in one the lateral order is rapidly lost as a function of distance and in the other the density has order only in the direction perpendicular to the interface, as it would in a liquid. Recently, Ohnesorge, Løwen, and Wagner [64] have presented a more flexible fully variational model that does not rely on shape functions; instead it determines the variation of the density directly from its Fourier representation. Both of the above mentioned approxima-

TABLE III. Summary of thermodynamic and structural information on the hard-sphere melt-solid interface.

Theory	(100) $\beta\gamma_{SL}d^2$	(100) Width	(111) $\beta\gamma_{SL}d^2$	(111) Width	(110) $\beta\gamma_{SL}d^2$	(110) Width
MC (this work)		$(4-5)d$		$(5-6)d$		$4d$
PGELA (CS) parametrization P-I	0.34	$3d$	0.37	$(3-4)d$	0.32	$3.3d$
PGELA (CS) parametrization P-II	0.35	$(4-5)d$	0.37	$(4-5)d$	0.33	$4d$
PGELA (PY) parametrization P-I	0.28	$4d$	0.30	$3.5d$	0.25	$4d$
PWDA [20]			0.60	$(3-4)d$		
WDA [18]	0.66	$(3-4)d$	0.63	$(3-4)d$		
WDA [64]	0.35	$5d$	0.26	$6d$	0.30	$4d$
MO-1 [15]	1.766	$(3-4)d$	1.762	$(3-4)d$	1.767	$(3-4)d$
MO-2 [16]			4.0	$\sim 6d$		

tions lead to much more computationally intensive calculations.

No Monte Carlo or molecular simulations exist for the surface free energy of the hard-sphere interface, so the accuracy of the predictions of the DFT cannot be tested directly. Comparison of results from various DFT approaches is complicated because each method is based on predictions corresponding to different solid-melt coexistence conditions and so the bulk densities used in each calculation are different. It is interesting that our predictions for the surface free energy using the PY equation of state are significantly smaller than previous results and are comparable to the recent predictions of Ohnesorge, Løwen, and Wagner [64]. For example, our values of γ_{SL} are approximately a factor of 2 smaller than the values predicted by Curtin [18] and Marr and Gast [20] based on the WDA and the PWDA free energy functionals. These differences cannot be attributed solely to the approximations for the excess free energy. The PGELA formulation of the free energy predicts for PY hard spheres a difference between the solid and liquid coexistence densities of $(\rho_s-\rho_l)d^3=0.097$, while both the PWDA and the WDA predict a difference of $(\rho_s-\rho_l)d^3=0.140$. Hence the density variation in the interfacial region is more abrupt with the WDA and larger excess properties should be expected. Another difference between the various theories is the degree of ordering predicted for the solid in equilibrium with the fluid phase. In most cases the theories overpredict the solid structure, thereby adding to the inaccuracy of the excess free energy prediction.

The ordering of the surface free energies for the crystallographic orientations of the interface also differs with the choice of DFT approximation; calculations with the WDA functional [18] predict that the (111) interface has a smaller surface free energy than the (100) interface, in contrast to our predictions using the PGELA DFT. The ordering predicted by Ohnesorge, Løwen, and Wagner [64] is that the (111) interface has the smallest surface free energy, followed by the (110) interface, which is also different from that found in this paper. The ordering of the surface free energies of these three orientations has been discussed by Broughton, Bonissent, and Abraham [34] and Stranski [65] and there is uncertainty as to whether the close-packed faces should have smaller or larger surface free energies than open faces. Stranski [65] argued that close-packed faces might be expected to have higher values of γ_{SL}. Our calculations seem to agree with this reasoning; however, the degree of anisotropy is found to be at the most about 10%. Interestingly, the molecular dynamics calculations of Broughton and Gilmer [19,35] demonstrated that the surface free energy is practically isotropic for the Lennard-Jones system, with very small differences in the free energies, leading to the order $(110)>(111)>(100)$. Clearly, the next steps are to calculate the surface free energy of the hard-sphere system by atomistic simulation [66] and to extend the density-functional thermodynamic perturbation scheme presented in Refs. [67,68] to the calculation of the melt-crystal system interface of the Lennard-Jones system.

ACKNOWLEDGMENT

The authors are grateful to the Microgravity Science and Application Program of NASA for support of this research.

[1] B. B. Laird and A. D. J. Haymet, Chem. Rev. **92**, 1819 (1992).
[2] D. P. Woodruff, *The Solid-Liquid Interface* (Cambridge University Press, London, 1973).
[3] N. Eustathopoulos, Int. Met. Rev. **28**, 189 (1983).
[4] K. A. Jackon, *Liquid Metals and Solidification* (ASM, Cleveland, 1958).
[5] D. E. Temkin, *Crystallization Processes* (Consultants Bureau, New York, 1964).
[6] J. F. Nicholas, Aust. J. Phys. **21**, 21 (1968).
[7] A. S. Skapski, Acta. Met. **4**, 576 (1956).
[8] S. N. Zadumkin, Fiz. Met. Metalloved. **13**, 24 (1962).
[9] A. D. J. Haymet and D. W. Oxtoby, J. Chem. Phys. **74**, 2559 (1981).
[10] D. W. Oxtoby and A. D. J. Haymet, J. Chem. Phys. **76**, 6262 (1982).
[11] W. H. Shih, Z. Q. Wang, X. C. Zeng, and D. Stroud, Phys. Rev. A **35**, 2611 (1987).
[12] X. C. Zeng and D. Stroud, J. Phys.: Condens. Matter **1**, 1779 (1989).
[13] X. C. Zeng, Phys. Chem. Liq. **20**, 39 (1989).
[14] S. M. Moore and H. J. Raveche, J. Chem. Phys. **85**, 6039 (1986).
[15] W. E. McMullen and D. W. Oxtoby, J. Chem. Phys. **88**, 1967 (1988).
[16] W. E. McMullen and D. W. Oxtoby, Phys. Chem. Liq. **18**, 97 (1988).
[17] W. A. Curtin, Phys. Rev. Lett. **59**, 1228 (1987).
[18] W. A. Curtin, Phys. Rev. B **39**, 6775 (1989).
[19] J. Q. Broughton and G. H. Gilmer, J. Chem. Phys. **84**, 5749 (1986).
[20] D. W. Marr and A. P. Gast, Phys. Rev. E **47**, 1212 (1993).
[21] J. P. Hansen and I. R. McDonald, *The Theory of Simple Liquids* (Academic, London, 1986).
[22] M. Baus and J. L. Colot, Phys. Rev. A **36**, 3912 (1987).
[23] A. Bonissent, in *Interfacial Aspects of Phase Transformations,* edited by B. Mutaftschiev (Reidel, Dordrecht, 1981), pp. 143–182.
[24] A. Bonissent and B. Mutaftschiev, CRC Crit. Rev. Solid State Mater. Sci. **10**, 297 (1981).
[25] O. A. Karim and A. D. J. Haymet, J. Chem. Phys. **89**, 6889 (1982).
[26] F. F. Abraham and J. Q. Broughton, Phys. Rev. Lett. **56**, 734 (1986).
[27] J. Q. Broughton and F. F. Abraham, J. Cryst. Growth **75**, 613 (1986).
[28] C. L. Cleveland, U. Landman, and R. N. Barnett, Phys. Rev. Lett. **49**, 790 (1982).

[29] E. Burke, J. Q. Broughton, and G. H. Gilmer, J. Chem. Phys. **89**, 1030 (1988).
[30] A. J. C. Ladd and L. V. Woodcock, Chem. Phys. Lett. **51**, 155 (1977).
[31] A. J. C. Ladd and L. V. Woodcock, Mol. Phys. **36**, 611 (1978).
[32] A. J. C. Ladd and L. V. Woodcock, J. Phys. C **11**, 3565 (1978).
[33] J. Q. Broughton and F. F. Abraham, Chem. Phys. Lett. **71**, 456 (1980).
[34] J. Q. Broughton, A. Bonissent, and F. F. Abraham, J. Chem. Phys. **74**, 4029 (1981).
[35] J. Q. Broughton and G. H. Gilmer, J. Chem. Phys. **84**, 5759 (1986).
[36] J. D. Bernal, Proc. R. Soc. London Ser. A **280**, 299 (1964).
[37] J. D. Bernal, I. A. Cherry, J. L. Finney, and K. R. Knight, J. Phys. E **3**, 388 (1970).
[38] A. Bonissent, in *Crystals 9* (Springer-Verlag, Berlin, 1983), pp. 1–21.
[39] J. Zell and B. Mutaftschiev, J. Cryst. Growth **13/14**, 231 (1972).
[40] A. Bonissent and B. Mutaftschiev, Philos. Mag. **35**, 65 (1977).
[41] G. Bushnell-Wye, J. L. Finney, and A. Bonissent, Philos. Mag. **44**, 1053 (1981).
[42] M. P. Allen and D. J. Tildesley, *Computer Simulation of Liquids* (Oxford University Press, New York, 1987).
[43] W. G. Hoover and F. H. Ree, J. Chem. Phys. **49**, 3609 (1968).
[44] I. K. Snook and D. Henderson, J. Chem. Phys. **68**, 2134 (1978).
[45] J. R. Henderson and F. Van Swol, Mol. Phys. **51**, 991 (1984).
[46] I. Snook and W. Van Megen, J. Chem. Phys. **70**, 3099 (1979).
[47] D. J. Courtemanche and F. Van Swol, Phys. Rev. Lett. **69**, 2078 (1992).
[48] A. Bonissent, E. Gauthier, and J. L. Finney, Philos. Mag. B **39**, 49 (1979).
[49] R. J. Galejs, H. J. Raveche, and G. Lie, Phys. Rev. A. **39**, 2574 (1989).
[50] R. Evans, Adv. Phys. **28**, 143 (1979).
[51] Y. Singh, Phys. Rep. **207**, 351 (1991).
[52] D. W. Oxtoby, in *Liquids, Freezing and the Glass Transition,* edited by J. P. Hansen, D. Levesque, and J. Zinn-Justin (Elsevier, Amsterdam, 1991).
[53] M. Baus, J. Phys.: Condens. Matter **2**, 2111 (1990).
[54] A. D. J. Haymet, Annu. Rev. Phys. Chem. **38**, 89 (1987).
[55] W. A. Curtin, J. Chem. Phys. **88**, 7050 (1988).
[56] J. F. Lutsko and M. Baus, Phys. Rev. A **41**, 6647 (1990).
[57] J. S. Rowlinson and B. Widom, *Molecular Theory of Capillarity* (Oxford University Press, New York, 1982).
[58] A. R. Denton and N. W. Ashcroft, Phys. Rev. A **39**, 4701 (1989).
[59] A. Kyrlidis and R. A. Brown, Phys. Rev. A **45**, 5654 (1992).
[60] W. A. Curtin and N. W. Ashcroft, Phys. Rev. A **32**, 2909 (1985).
[61] D. W. Marr (private communication).
[62] A. Kyrlidis, Ph.D. thesis, Massachusetts Institute of Technology, 1993.
[63] L. Mikheev and A. Trayanov, Surf. Sci. **223**, 299 (1989).
[64] R. Ohnesorge, H. Løwen, and H. Wager (unpublished).
[65] I. N. Stranski, Naturwissenschaften **30**, 425 (1942).
[66] Y. V. Naidich, N. F. Grigorenko, and V. M. Perevertailo, J. Cryst. Growth **53**, 261 (1981).
[67] A. Kyrlidis and R. A. Brown, in *Computational Methods in Materials Science,* edited by J. E. Mark, M. E. Glicksman, and S. P. Marsh, MRS Symposia Proceedings No. 278 (Materials Research Society, Pittsburgh, 1992), pp. 21–26.
[68] A. Kyrlidis and R. A. Brown, Phys. Rev. E **47**, 427 (1993).